View metadata, citation and similar papers at core.ac.uk

brought to you by CORE

provided by Radboud Repository

Radboud Repository

Radboud University Nijmegen

PDF hosted at the Radboud Repository of the Radboud University Nijmegen

The following full text is a publisher's version.

For additional information about this publication click this link.
http://hdl.handle.net/2066/177957

Please be advised that this information was generated on 2018-07-07 and may be subject to change.

This is an open access article published under a Creative Commons Non-Commercial No Derivative Works (CC-BY-NC-ND) Attribution License, which permits copying and redistribution of the article, and creation of adaptations, all for non-commercial purposes.

JOC The Journal of Organic Chemistry

Article

pubs.acs.org/joc

Stabilization of 2,6-Diarylanilinum Cation by Through-Space Cation–π Interactions

Joan Simó Padial,[†,⊥] Jordi Poater,[‡,§,⊥] D. Thao Nguyen,[†] Paul Tinnemans,[†] F. Matthias Bickelhaupt,*[,†,∥] and Jasmin Mecinović*[,†]

[†]Institute for Molecules and Materials, Radboud University, Heyendaalseweg 135, 6525 AJ Nijmegen, The Netherlands

[‡]Catalan Institution for Research and Advanced Studies (ICREA), Passeig Lluís Companys 23, 08010 Barcelona, Spain

[§]Departament de Química Inorgànica i Orgànica and IQTCUB, Universitat de Barcelona, Martí i Franquès 1-11, 08028 Barcelona, Spain

[∥]Department of Theoretical Chemistry, Amsterdam Center for Multiscale Modeling, Vrije Universiteit Amsterdam, De Boelelaan 1083, 1081 HV Amsterdam, The Netherlands

Supporting Information

ABSTRACT: Energetically favorable cation–π interactions play important roles in numerous molecular recognition processes in chemistry and biology. Herein, we present synergistic experimental and computational physical–organic chemistry studies on 2,6-diarylanilines that contain flanking *meta*/*para*-substituted aromatic rings adjacent to the central anilinium ion. A combination of measurements of pK_a values, structural analyses of 2,6-diarylanilinium cations, and quantum chemical analyses based on the quantitative molecular orbital theory and a canonical energy decomposition analysis (EDA) scheme reveal that through-space cation–π interactions essentially contribute to observed trends in proton affinities and pK_a values of 2,6-diarylanilines.

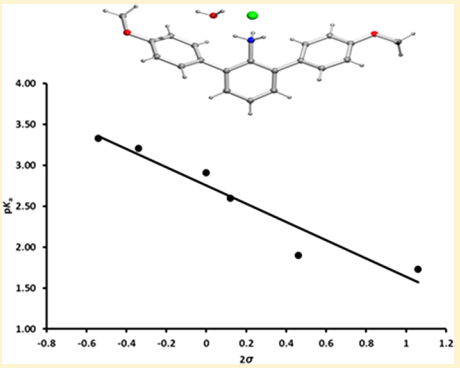

INTRODUCTION

The qualitative and quantitative examination of weak noncovalent interactions in chemical and biological systems has been a focus area of modern chemistry, ranging from physical–organic and supramolecular chemistry to medicinal chemistry and chemical biology.[1] In biological molecular recognitions, the aromatic rings play the essential role in stabilization of protein structure and in specific interactions between proteins and their substrates, co-substrates, and inhibitors.[1d,2] Biostructural analyses of proteins in their free and complexed forms revealed that the electron-rich aromatic rings that constitute the side chains of phenylalanine, tyrosine, and tryptophan have the ability to participate in various noncovalent interactions, including cation–π interactions, π–π interactions, sulfur–π interactions, and hydrogen bonding.[1d,2c,3]

Quantifying the energetics of intermolecular interactions between aromatic rings and polar functional groups, including the positively charged functionalities (i.e., cation–π interactions), in biology remains a challenge, thus several simpler small molecule host–guest systems have been developed for this purpose.[1a,4] The simplest molecular systems, however, could in principle be based on molecular architectures in which intramolecular interactions are structurally and energetically examined between the cationic moiety and the aromatic ring that are part of the same molecule. In order to provide an advanced understanding of the nature of noncovalent interactions within small molecules, the physical–organic chemistry approaches enabled compelling experimental and computational investigations of intramolecular polar–π interactions that are present in 2,6-diarylpyridines,[5] (2,6-pyridino)-paracyclophanes,[6] 2,6-diarylphenyldimethylsilyl cations,[7] and 2,6-diarylbenzoic acids[8] (Figure 1). Herein, we report physical–organic chemistry studies on 2,6-diarylanilines and associated 2,6-diarylanilinium ions that provide strong evidence for the existence of stabilizing through-space cation–π interactions between the central anilinium cation and the two neighboring aromatic rings.

RESULTS AND DISCUSSION

Early physical–organic chemistry investigations, based on Hammett analysis, on *para*-substituted anilines revealed that through-bond inductive and resonance (mesomeric) effects importantly contribute to their strength of basicity and nucleophilic character.[9] The influence of through-space effects on the basicity of anilines, however, has not been explored in detail.[10] We envisioned that 2,6-diarylanilinium ions possess a proper structural arrangement that allows us to examine the nature and the effect of through-space noncovalent interactions on chemical properties of 2,6-diarylanilines (Figure 1). We

Received: June 7, 2017
Published: August 24, 2017

 © 2017 American Chemical Society

DOI: 10.1021/acs.joc.7b01406
J. Org. Chem. 2017, 82, 9418–9424

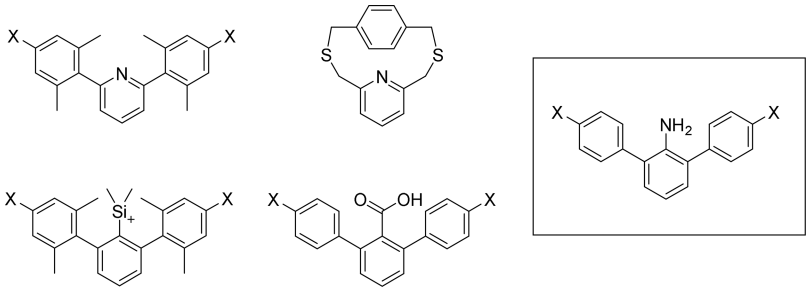

Figure 1. 2,6-Diaryl-substituted aromatic systems for studies of through-space interactions. The 2,6-diarylaniline scaffold used in this study is shown in the box on the right.

hypothesized that there is a linear dependence of the basicity of *para*-substituted 2,6-diarylanilines on the Hammett σ values and that such linear trends are not caused by through-bond orbital interactions, but rather by mechanistically distinct through-space orbital interactions.

Para- and *meta*-substituted 2,6-diarylanilines **1**–**8** were synthesized in good yields from 2,6-dibromoaniline and *para*/*meta*-substituted phenylboronic acids employing the palladium-catalyzed Suzuki cross-coupling reaction (Scheme 1).

Scheme 1. Synthesis of 2,6-Diarylanilines 1–8 under Suzuki Cross-Coupling Conditions

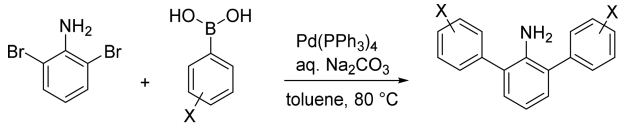

We measured pK_a values for anilines **1**–**8** in aqueous solutions (with 4% methanol) employing an established UV–vis spectroscopy-based method (Table 1).[11] The observed p*K*a values were then plotted against the Hammett σ values ($2\sigma_{para}$, because there are two flanking aromatic rings adjacent to the pivotal aniline ring, each having one substituent at the *para* position). As shown in Figure 2, it is evident that there is a clear linear correlation ($R^2 > 0.92$) between the acidity constants of *para*-substituted 2,6-diarylanilines **1**–**6** and the Hammett σ values. The ρ value for the tested series of anilines **1**–**6** was observed to be +1.1, implying that the acidity of anilines is sensitive to *para*-substituents at the flanking aromatic rings and that, as expected, the positive charge is lost during deprotonation. In this regard, virtually the same ρ value was observed for the series of analogous 2,6-diarylpyridines.[5] The presence of the electron-donating groups (e.g., OMe) leads to a weaker acidity of the anilinium ion (and stronger basicity of the aniline); the observation that could be attributed to through-space stabilization of anilinium ion by the electron-rich aromatic rings. Accordingly, the presence of the electron-withdrawing groups (e.g., CF_3) makes the anilinium ion a significantly stronger acid.

Table 1. pK_a Values for Anilines 1–8

compd	X	σ	pK_a[a]
1	H	0.00	2.97
2	*p*-OMe	−0.27	3.33
3	*p*-Me	−0.17	3.21
4	*p*-F	0.06	2.60
5	*p*-Cl	0.23	1.90
6	*p*-CF_3	0.54	1.78
7	*m*-OMe	0.12	3.26
8	*m*-F	0.34	2.53

[a]Determined in H_2O:MeOH = 96:4

It is noteworthy that substituents at the *meta* and *para* positions of the flanking rings that exhibit significantly different σ_{meta} and σ_{para} values do not substantially alter the pK_a values of such anilines (Table 1). We chose OMe and F substituents, respectively, to examine the effect of the position of the substituent at the flanking aromatic rings on the basicity of 2,6-diarylanilines due to the fact that these two substituents exhibit significantly different Hammett values when placed on the *meta* and *para* positions and are presumably the best examples of common substituents to address the nature of interactions employing physical–organic chemistry approaches. For instance, the *meta*-substituted OMe (**7**) and its *para*-substituted counterpart (**2**) have very similar pK_a values (3.26 vs 3.33), despite having significantly different σ values (0.12 vs −0.27). Similarly, although the *meta*-substituted F (**8**) and the *para*-substituted F (**4**) differ in their σ values (0.34 vs 0.06), they do have comparable pK_a values of 2.53 and 2.60, respectively. Collectively, these results imply that through-bond effects (induction and/or resonance) do not account for the observed trends in pK_a values of 2,6-diarylanilines. Instead, based on our Hammett plot analysis and comparison of pK_a values of *meta*/*para*-substituted 2,6-diarylanilines, it is most likely that through-space cation–π interactions between the central anilinium ion and the two neighboring flanking aromatic rings contribute to the strength of the basicity of 2,6-diarylanilines via different degrees of stabilization of their conjugated 2,6-diarylanilinium ions.

Having shown that *para*-substituents at the flanking aromatic ring affect the pK_a values of 2,6-diarylanilines in a predictive manner, we then carried out X-ray crystallographic studies with the aim of providing the structural information about the 2,6-diarylanilinium ion. We solved crystal structures of **2**·HCl and **2**·$HClO_4$ in high-resolution; the needle-shaped crystals were grown in ethanol at 4 °C.[12] For both complexes, dihedral angles between the central anilinium ion and the adjacent aromatic rings were observed to be 50–60° (Figures 3 and S1–2). Both flanking aromatic rings exhibit the "parallel" or "eclipsed" orientation, thus allowing two hydrogens of the middle anilinium NH_3^+ to associate with electron-rich aromatic rings (Figure 3). Structural analyses revealed that the average distances between the closest anilinium N–H$^+$ hydrogens and carbon atoms of the adjacent flanking rings are NH-C_α 2.6 Å, NH-C_β 2.7 Å, NH-C_γ 3.7 Å, and NH-C_δ 4.5 Å. The remaining third N–H$^+$ hydrogen of the anilinium NH_3^+ functionality

DOI: 10.1021/acs.joc.7b01406
J. Org. Chem. 2017, 82, 9418–9424

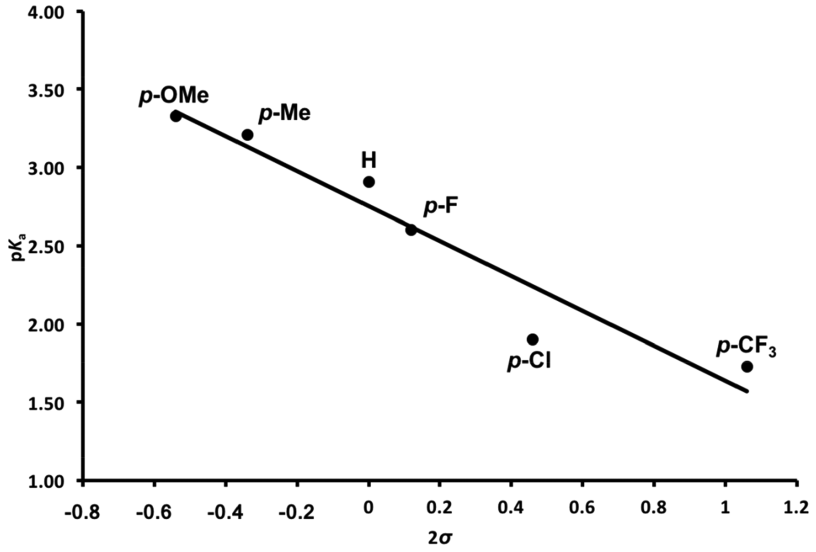

Figure 2. Dependence of pK_a values of *para*-substituted anilines **1**–**6** on the Hammett σ values. 2σ is the sum of the Hammett σ values of *para*-substituents on both flanking rings.

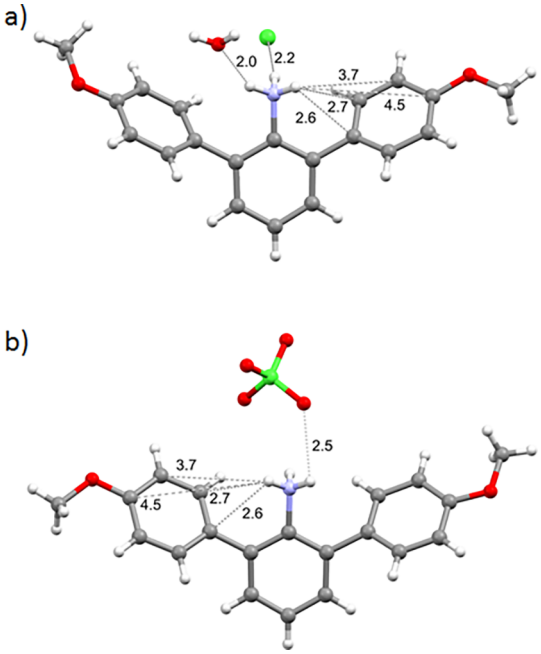

Figure 3. Views on the crystal structures of (a) **2**·HCl and (b) **2**·$HClO_4$. Important distances (in Å) between hydrogens of the NH_3^+ group and the surrounding atoms are shown.

forms the electrostatic interaction with the counterion. The distance between N–H^+ and Cl^- is 2.2 Å, whereas the distance between N–H^+ and the closest oxygen of ClO_4^- was measured to be 2.5 Å (Figure 3). In addition, in the **2**·HCl structure, a water molecule was observed in close proximity (2.0 Å) to one of the anilinium N–H^+ hydrogens that interacts with the flanking aromatic rings (Figure 3).

With the aim of providing a more advanced understanding of the molecular origin for the observed trends of pK_a values of 2,6-diarylanilines, we then carried out computational studies with basic 2,6-diarylanilines and their corresponding conjugate acids. All calculations were performed with the Amsterdam Density Functional (ADF) program[13] using relativistic density functional theory (DFT) at ZORA-BP86/TZ2P for geometry optimization and energy calculations.[14] The effect of aqueous solvation was simulated by means of the Conductor like Screening Model (COSMO) of solvation as implemented in ADF.[15] The energetically most favorable conformations of the 2,6-diarylanilnium ions **1**–**8** appear at the dihedral angles of 55–58° (Table S1). The calculated dihedral angles (NC–C_2–C_α–C_β) for the most stable conformers are in very good agreement with our crystallographically obtained structures of **2**·HCl and **2**·$HClO_4$. Moreover, the lowest-energy conformers also possess similar distances to the neighboring aromatic rings as obtained by the determined crystal structures. Furthermore, computational analyses of the most stable conformers illustrate, in line with structural information, that both flanking rings of 2,6-diarylanilnium ions **1**–**8** exhibit the approximate "parallel" or "eclipsed" geometry, that is, both flanking rings are on the same side with respect to the central anilinium cation. This differs from the situation that we found in earlier structural and computational work for the related 2,6-diarylpyridinium ions, in which case we verified that both flanking rings possess the "antiparallel" or "staggered" conformation.[5]

The rotation barrier was then calculated for the anilinium cation **1** in the range from 0° to 180°. In line with the crystallographic studies and the optimization of the lowest-energy conformer, rotational barrier analyses confirmed that the energetically most stable structure of cationic **1** possesses the dihedral angle of 58° (Figure 4; note: only one Ar–Ar dihedral angle is varied, whereas another Ar–Ar dihedral angle is kept fixed at 58°). As clearly seen in Figure 4, conformations with dihedral angles below 35° are at relatively high energy. Notably, the most unstable structure of the anilinium cation **1** occurs at dihedral angle of 0°. On the other hand, conformers with dihedral angles in the interval between 40° and 130° differ <1 kcal mol^{-1} in their relative energy ΔE, suggesting that multiple conformations could coexist in solution. Again, the rotation barrier graph for the 2,6-diarylanilinium cation well resembles the computed rotation barriers for the analogous 2,6-diarylpyridinium cations.[5]

Next, we calculated proton affinities (PA) for 2,6-diarylanilines **1**–**8** in the gas phase and in aqueous solution using COSMO (Table 2). Proton affinity energies (ΔE^{PA}) of anilines **1**–**6** were plotted against the 2σ of *para*-substituents at flanking

DOI: 10.1021/acs.joc.7b01406
J. Org. Chem. 2017, 82, 9418–9424

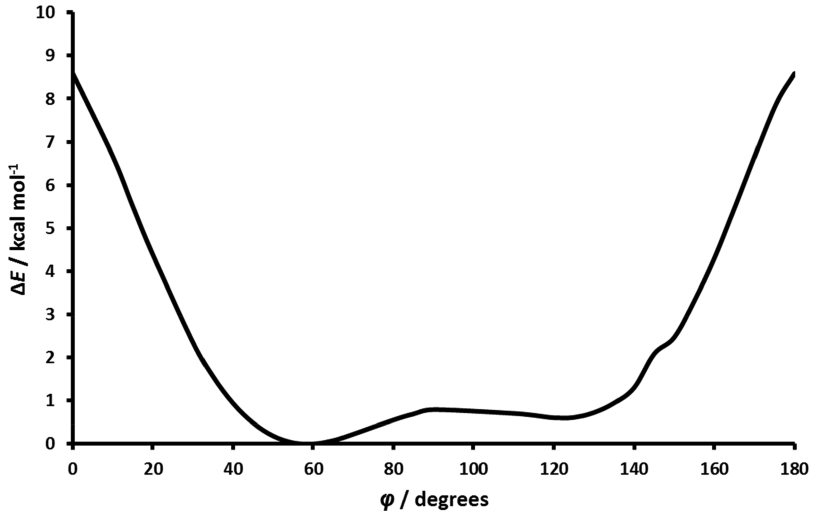

Figure 4. Dependence of the relative energy ΔE of anilinum cation **1** on the dihedral angle φ, computed at BP86/TZ2P.

Table 2. Proton Affinity Energies ΔE^{PA} (in kcal mol^{-1}) for Anilines 1−8 Computed at ZORA-BP86/TZ2P

compd	X	ΔE^{PA} in gas phase	ΔE^{PA} in water[a]
1	H	227.2	149.8
2	*p*-OMe	231.2	150.0
3	*p*-Me	230.0	150.0
4	*p*-F	222.8	149.4
5	*p*-Cl	222.3	149.6
6	*p*-CF_3	217.4	148.0
7	*m*-OMe	230.7	150.2
8	*m*-F	222.8	148.9

[a]Solvation in water was simulated using COSMO.

aromatic rings (Figure 5). In the gas phase, the data evidently showcase a strong linear relationship between the ΔE^{PA} and 2σ with the slope of −8.8 ($R^2 > 0.94$). In water, the trend is also linear ($R^2 > 0.84$), but the slope of −1.2 is significantly less negative relative to the one in the gas phase. The values of the slopes indicate that, as expected, the proton affinities of 2,6-diarylanilines are substantially more affected in the gas phase than in water by the substituents at the flanking aromatic rings. Moreover, the comparison of ΔE^{PA} values of *meta*- and *para*-substituted OMe and F, respectively, highlights comparable proton affinity energies, despite very different values of 2σ for *meta*- and *para*-substituents, again implying that through-space interactions play a dominant role in the stabilization of 2,6-diarylanilinium ions. Taken together, the signature of calculated proton affinity energies is in good agreement with the trend of measured pK_a values of anilines **1**−**8**; both undoubtedly show that the strength of basicity is highly dependent on the electron-donating/electron-withdrawing properties of substituents located at the distant *meta* and *para* positions of the flanking aromatic rings.

We then carried out more detailed analyses on the origin of the *para*-substituent effect on the PA of 2,6-diarylanilines **2** and **6** that possess the OMe and CF_3 substituents, respectively. The two substituents represent the opposite extremes along the series of substituents that were investigated: *para*-OMe substitution leads to the largest proton affinity (231.2 kcal mol^{-1}), whereas *para*-CF_3 substitution results in the lowest proton affinity (217.4 kcal mol^{-1}). Such a difference is attributed to different electron-donating/electron-withdrawing

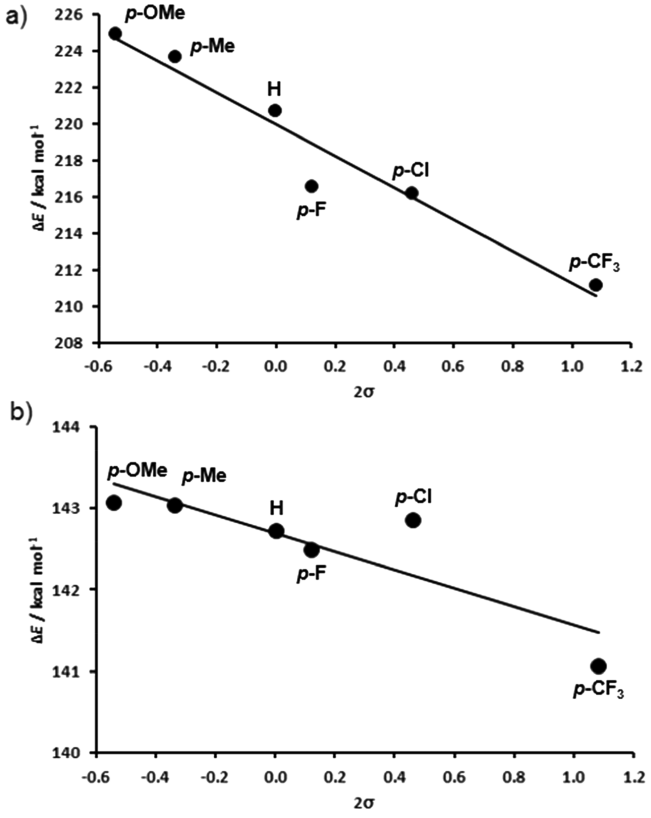

Figure 5. Dependence of proton affinity energies (ΔE) in the gas phase (a) and in water (b) on the Hammett σ values of *para*-substituted anilines **1**−**6**.

character of these two substituents, with values of Hammett σ constants (2σ) being −0.54 for OMe and 1.08 for CF_3. Thus, OMe makes the anilinium ring significantly more basic than does CF_3. Our work also shows that the OMe substituent placed at the *meta* position results in a similar PA (−230.7 kcal mol^{-1}), despite having a very different 2σ value of 0.24. Thus, we have included *meta*-substituted anilinium cation in our further analyses.

We focused again on those systems that have the largest and the smallest proton affinity in our series, including electron-donating and electron-withdrawing groups. Thus, the following

DOI: 10.1021/acs.joc.7b01406
J. Org. Chem. 2017, 82, 9418−9424

analysis was performed on *para*-CF_3- and *para*-OMe-substituted 2,6-diarylanilinium systems (pCF_3_H^+ and pOMe_H^+, respectively). In order to analyze the through-space interactions between the ammonium group and the two *para*-substituted aryl rings in the anilinium cations, the central benzene ring was removed, while the remaining three moieties (two *para*-substituted phenyl radicals and the ammonia radical cation) were kept frozen to their geometry and position they had in the complete anilinium system (see Figure 6). The

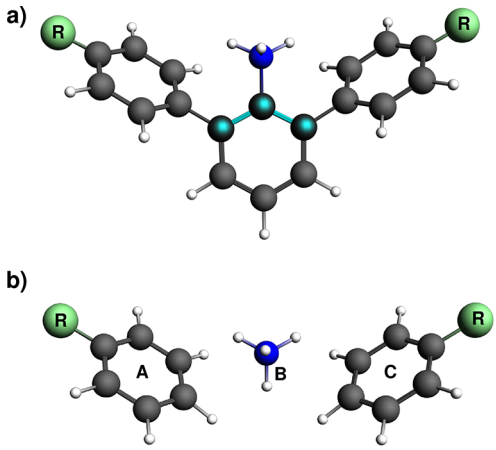

Figure 6. Structure of (a) *para*-substituted 2,6-diarylanilinium cation and (b) mode system used in through-space cation–π interaction analysis.

radical positions were terminated with hydrogen atoms (see the three light blue atoms in Figure 6a). Note that only these three hydrogen atoms were geometrically optimized at the ZORA-BP86/TZ2P level (see Figure 6b); the rest of the system was kept frozen in order to keep the structure of the original system.

We have analyzed: (i) the interaction between the two substituted benzene rings A and C upon formation of [A···C] and (ii) the interaction between this [A···C] fragment and B = NH_4^+ or NH_3. The interaction energy ΔE_{int} between the phenyl rings A and C in [A···C] is slightly repulsive but close to zero (Table 3), due to the long distance between them (closest H···H distance is 3.2 Å).

Next, the through-space cation–π interaction of the [A···C] fragment with the ammonium fragment B was subject to a bonding analysis including the energy decomposition energy (EDA). First, the interaction ΔE_{int} in the case of the OMe (pOMe_H^+) substituent (−17.5 kcal mol^{-1}) is clearly more stabilizing than in the case of the CF_3 (pCF_3_H^+) substituent (−3.3 kcal mol^{-1}; see Table 3). This is the source of the higher PA of the *para*-OMe-substituted diarylaniline system, given the fact that the through-space neutral N–H–π interaction in the corresponding unprotonated diaryl aniline **2** is repulsive and approximately equal in the case of the two substituents (i.e., 7–8 kcal mol^{-1}; see Table 3).

The EDA decomposition of ΔE_{int} into electrostatic, Pauli, and orbital interaction terms allowed us to assign such difference to ΔV_{elstat}, which is reduced from −18.5 to −2.4 kcal mol^{-1} as we go from pOMe_H^+ to pCF_3_H^+. On the other hand, ΔE_{Pauli} and ΔE_{oi} present similar magnitudes for both substituents (Table 3). With the aim to understand the different magnitudes in electrostatic interaction from OMe to CF_3, the Voronoi deformation density (VDD) charges were then calculated. Figure 7 depicts the VDD charges for both substituted [A···C] fragments for either pCF_3_H^+ (Figure 7a) or pOMe_H^+ (Figure 7c) systems. The latter causes the carbon atoms of the benzene ring to be more negatively charged than those in the presence of CF_3. Note the exception of the C atom directly linked to OMe, which experiences an inductive effect. In fact, the overall charge of the aryl ring with pCF_3_H^+ is +30 me., compared to −18 me. for pOMe_H^+. This trend in aryl ring charge reflects the electron-pushing character of OMe and the electron-pulling character of CF_3. The more negatively charged pOMe-substituted aryl rings enter into a more stabilizing electrostatic interaction ΔV_{elstat} with the ammonium cation (Figure 7b), as revealed by our EDA analysis (Table 3). It is noteworthy that Wheeler's and Houk's computational results suggest that substituent effects in cation–π interactions and π–π stacking interactions could arise mainly from direct interactions of the cation with the substituents, whereas π polarization seems to only play a minor role.[3,16] Our 2,6-diarylanilinium system, however, possesses the geometry in which the substituents at the distant *para*/*meta*-positions of the flanking aromatic rings are located away from the anilinium cation and therefore cannot participate in energetically favorable direct interactions with the NH_3^+ functionality.

The magnitude of the through-space orbital interactions is very similar for the pCF_3_H^+ and pOMe_H^+ anilinium cations, namely, − 26.3 and −27.3 kcal mol^{-1}, respectively (Table 3). The dominant frontier orbitals in this interaction are the symmetric combination of the aromatic π-type HOMOs of the two aryl groups in the [A···C] fragment and the unoccupied N–H σ* LUMO of the ammonium cation (see Figure 8). Note that the substituents affect the shape of the aryl HOMO only marginally, as reflected also by the moderate change in overlap values (Figure 8). As a consequence, if all pairs of donor–acceptor orbital interactions as well as closed-shell–closed-shell repulsions are taken together (not all shown in Figure 8), the

Table 3. Through-Space Cation–π Interaction Analyses (in kcal mol^{-1}) for the Modified Anilinium Cation (B = NH_4^+) and Aniline (B = NH_3) Model Systems[a]

			A + C → [A···C]	[A···C] + B → [A···B···C]			
system	R	B	ΔE_{int}	ΔE_{int}	ΔE_{Pauli}	ΔV_{elstat}	ΔE_{oi}
pCF_3_H^+	CF_3	NH_4^+	0.4	−3.3	25.4	−2.4	−26.3
pOMe_H^+	OMe	NH_4^+	0.3	−17.5	28.3	−18.5	−27.3
mOMe_H^+	OMe	NH_4^+	0.3	−17.7	29.7	−18.4	−29.0
pCF_3	CF_3	NH_3	0.5	7.1	21.8	−9.4	−5.3
pOMe	OMe	NH_3	0.3	7.8	24.6	−10.9	−5.8
mOMe	OMe	NH_3	0.3	7.8	24.0	−10.4	−5.8

[a]See Figure 6b. Computed at the ZORA-BP86/TZ2P level of theory.

DOI: 10.1021/acs.joc.7b01406
J. Org. Chem. 2017, 82, 9418–9424

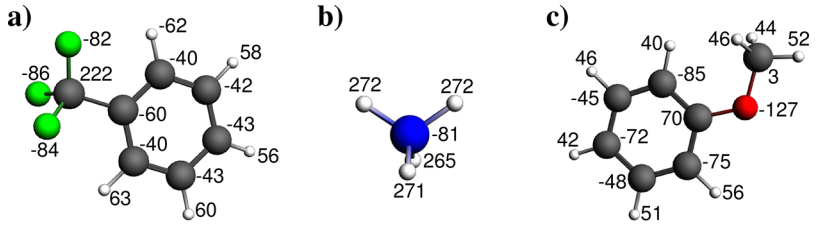

Figure 7. VDD charges (in milli-electrons) for fragments (a) pCF$_3$_H$^+$ in [A···C]; (b) NH$_4^+$; and (c) pOMe_H$^+$ in [A···C], calculated at ZORA-BP86/TZ2P level.

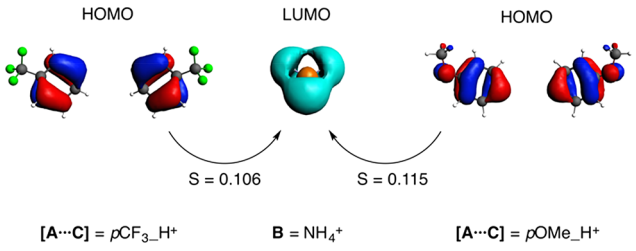

Figure 8. HOMOs of the pCF$_3$- (left) and pOMe-substituted (right) diaryl fragment [A···C] and LUMO orbital of B = ammonium cation (center) showing the relevant HOMO−LUMO overlap.

effects are marginal, and the ΔE_{oi} and ΔE_{Pauli} terms change only insignificantly along the different substituents. Therefore, even though they constitute a large bonding term, the orbital interactions are not responsible for the difference in through-space interaction and thus PA between pCF$_3$- and pOMe-substituted anilines. This difference originates from the significantly different electrostatic attraction ΔV_{elstat}.

Finally, we have also performed the EDA analysis for *meta*-OMe-substituted 2,6-diarylanilinium (mOMe_H$^+$). The results enclosed in Table 3 confirm indeed similar behavior of this substituent either at the *meta*- or *para*-position in the aryl rings with respect to its proton affinities. This is further and direct evidence that the mechanism behind the substituent effect on the PA is a through-space interaction.

CONCLUSIONS

In conclusion, we have demonstrated that pK_a values and proton affinities of 2,6-diarylanilines undergo linear correlation with respect to Hammett σ values of substituents at the distant *para* position of the flanking aromatic rings. We attribute these observed and calculated trends to through-space cation−π interactions between the central anilinium cation and the two neighboring, electron-rich aromatic rings. Our compelling experimental and computational work shows that through-bond effects do not account for the observed strengths of basicity for a series of 2,6-diarylanilines. A nonplanarity of the system highlights that the resonance effect does not play an important role in the chemical properties of 2,6-diarylanilines. The inductive effect is also excluded due to a presence of several bonds (six bonds between the anilinium NH$^+$ and the substituted C$_\delta$ of the flanking aryl rings). Our experimental investigations are strongly supported by quantitative MO theory and energy decomposition analyses that conclusively provide evidence that (i) the effect of the *para*-substituents is through-space; (ii) through-space orbital interactions are sizable but do not discriminate; and (iii) instead it is the electrostatic attraction between the electron-rich aromatic rings and the positively charged ammonium ion that is decisive for the trend in proton affinity values. In association with recent examinations of energetically favorable cation−π interactions in biomolecular systems,[17] we showcase that our physical−organic approach provides a strong support for the stabilization of 2,6-diarylanilinium cations via intramolecular through-space cation−π interactions.

EXPERIMENTAL SECTION

Synthesis of 2,6-Diarylanilines. To a stirred solution of 2,6-dibromoaniline (0.5 mmol) and Pd(PPh$_3$)$_4$ (0.08 mmol) in toluene (7 mL) were added the ethanolic solution of arylboronic acid (0.75 M, 1.5 mmol) and the aqueous solution of Na$_2$CO$_3$ (1.87 M, 4 mL). The reaction mixture was then stirred at 80 °C for 3 days. The solution was poured into 30 mL of water and extracted with diethyl ether (3 × 30 mL). Combined organic layers were then dried with Na$_2$SO$_4$, filtered, and evaporated *in vacuo*. The crude product was purified by column chromatography (5% ethyl acetate, 95% heptane) to afford pure 2,6-diarylaniline.

1: White solid (94 mg, 77% yield); mp 83−85 °C; ^{1}H NMR (500 MHz, CDCl3) δ 7.52−7.50 (m, 4H), 7.47−7.44 (m, 4H), 7.37−7.34 (m, 2H), 7.12 (d, J = 7.5 Hz, 2H), 6.90−6.87 (m, 1H), 3.84 (s, 2H); ^{13}C NMR (126 MHz, CDCl$_3$) δ 140.8, 139.8, 129.8, 129.3, 128.9, 127.9, 127.3, 118.1; HRMS (ESI-TOF) m/z: [M + H]$^+$ calcd for C$_{18}$H$_{16}$N 246.1277; found 246.1286.

2: White solid (105 mg, 69% yield); mp 102−104 °C; ^{1}H NMR (500 MHz, CDCl$_3$) δ 7.45−7.42 (m, 4H), 7.08 (d, J = 7.5 Hz, 2H), 7.00−6.98 (m, 4H), 6.88−6.83 (m, 1H), 3.85 (s, 6H), 3.81 (s, 2H); ^{13}C NMR (126 MHz, CDCl$_3$) δ 158.8, 141.2, 132.0, 130.4, 129.5, 127.6, 118.1, 114.2, 55.3; HRMS (ESI-TOF) m/z: [M + H]$^+$ calcd for C$_{20}$H$_{20}$NO$_2$ 306.1489; found 306.1493.

3: White solid (96 mg, 70% yield); mp 115−116 °C; ^{1}H NMR (500 MHz, CDCl$_3$) δ 7.45−7.43 (m, 4H), 7.30−7.28 (m, 4H), 7.13 (d, J = 7.5 Hz, 2H), 6.92−6.89 (m, 1H), 3.51 (s, 2H), 2.42 (s, 6H); ^{13}C NMR (126 MHz, CDCl$_3$) δ 156.1, 143.9, 143.7, 141.3, 127.7, 127.1, 125.1, 120.0, 29.4; HRMS (ESI-TOF) m/z: [M + H]$^+$ calcd for C$_{20}$H$_{20}$N 274.1590; found 274.1592.

4: White solid (62 mg, 44% yield); mp 145−146 °C; ^{1}H NMR (500 MHz, CDCl$_3$) δ 7.74−7.63 (m, 4H), 7.14 (d, J = 7.5 Hz, 2H), 6.94−6.91 (m, 2H), 3.78 (s, 2H); ^{13}C NMR (126 MHz, CDCl$_3$) δ 162.1 (d, J = 247 Hz), 140.9, 135.5 (d, J = 3.5 Hz), 131.0 (d, J = 8.0 Hz), 129.9, 127.0, 118.2, 115.8 (d, J = 21.5 Hz).; HRMS (ESI-TOF) m/z: [M + H]$^+$ calcd for C$_{18}$H$_{14}$F$_2$N 282.1089; found 282.1095.

5: White solid (99 mg, 63% yield); mp 111−113 °C; ^{1}H NMR (500 MHz, CDCl$_3$) δ 7.48−7.45 (m, 4H), 7.17−7.12 (m, 4H), 7.09 (d, J = 7.5 Hz, 2H), 6.87 (t, J = 7.5 Hz, 1H), 3.75 (s, 2H); ^{13}C NMR (126 MHz, CDCl$_3$) δ 140.6, 137.9, 133.3, 130.7, 129.9, 129.1, 126.8, 118.4; HRMS (ESI-TOF) m/z: [M + H]$^+$ calcd for C$_{18}$H$_{14}$Cl$_2$N 314.0498; found 314.0515.

6: White solid (145 mg, 76% yield); mp 79−81 °C; ^{1}H NMR (500 MHz, CDCl$_3$) δ 7.74−7.63 (m, 8H), 7.14 (d, J = 7.5 Hz, 2H), 6.93 (t, J = 7.5 Hz, 1H), 3.78 (s, 2H); ^{13}C NMR (126 MHz, CDCl$_3$) δ 143.2, 140.5, 130.3, 129.6 (q, J = 32.5 Hz), 129.5, 126.7, 125.9 (q, J = 3.5 Hz), 124.1 (q, J = 272.0 Hz), 118.6; HRMS (ESI-TOF) m/z: [M + H]$^+$ calcd for C$_{20}$H$_{14}$F$_6$N 382.1025; found 382.1028.

7: White solid (113 mg, 74% yield); mp 113−114 °C; ^{1}H NMR (500 MHz, CDCl$_3$) δ 7.38−7.35 (m, 2H), 7.12 (d, J = 7.5 Hz, 2H), 7.10−7.08 (m, 2H), 7.05−7.04 (m, 2H), 6.92−6.90 (m, 2H), 6.88−

DOI: 10.1021/acs.joc.7b01406
J. Org. Chem. 2017, 82, 9418−9424

6.84 (m, 1H), 3.92 (s, 2H), 3.84 (s, 6H); ^{13}C NMR (126 MHz, $CDCl_3$) δ 159.9, 141.1, 140.8, 129.9, 129.7, 127.7, 121.6, 117.9, 114.7, 113.1, 55.3; HRMS (ESI-TOF) m/z: $[M + H]^+$ calcd for $C_{20}H_{20}NO_2$ 306.1489; found 306.1497.

8: White solid (65 mg, 46% yield); mp 58−59 °C; ^{1}H NMR (500 MHz, $CDCl_3$) δ 7.44−7.41 (m, 2H), 7.29−7.27 (m, 2H), 7.23−7.20 (m, 2H), 7.12 (d, J = 7.5 Hz, 2H), 7.06 (m, 2H), 6.88 (t, J = 7.5 Hz, 1H), 4.30−3.46 (bs, 2H); ^{13}C NMR (126 MHz, $CDCl_3$) δ 163.1 (d, J = 247 Hz), 141.7, 130.5 (d, J = 7.5 Hz), 130.0, 126.8, 125.0, 118.3, 116.3 (d, J = 7.5 Hz), 114.4, 114.2; HRMS (ESI-TOF) m/z: $[M + H]^+$ calcd for $C_{18}H_{14}F_2N$ 282.1089; found 282.1091.

Quantum Chemical Analyses. The bonding mechanism of ammonium cation (taken from the anilinium cation) or ammonia (taken from aniline) with the two substituted benzene rings (taken from aryl rings) was analyzed within the framework of quantitative Kohn−Sham molecular orbital theory[18] in combination with a quantitative energy decomposition analysis (EDA)[18] in the gas phase. The electronic bond energy ΔE can be decomposed into the strain energy ΔE_{strain} associated with deforming the fragments from their equilibrium structure to the geometry they adopt in modified aniline, plus the interaction energy ΔE_{int} between these deformed fragments. The latter is further decomposed into the classical electrostatic attraction ΔV_{elstat}, Pauli repulsion ΔE_{Pauli} between occupied orbitals, and stabilizing orbital interactions ΔE_{oi}.[14a−c,e] Atomic charges were computed with the Voronoi deformation density (VDD) method.[19]

■ ASSOCIATED CONTENT

Supporting Information

The Supporting Information is available free of charge on the ACS Publications website at DOI: 10.1021/acs.joc.7b01406.

NMR spectra, pK_a measurements, X-ray crystallography data, computational studies (PDF)

Crystallographic data for **2**·HCl (CIF)

Crystallographic data for **2**·$HClO_4$ (CIF)

■ AUTHOR INFORMATION

Corresponding Authors

*E-mail: j.mecinovic@science.ru.nl.

*E-mail: f.m.bickelhaupt@vu.nl

ORCID

F. Matthias Bickelhaupt: 0000-0003-4655-7747

Jasmin Mecinović: 0000-0002-5559-3822

Author Contributions

⊥These authors contributed equally to this work.

Notes

The authors declare no competing financial interest.

■ ACKNOWLEDGMENTS

We thank The Netherlands Organization for Scientific Research (NWO) for financial support. J.P. thanks the Spanish MINECO (CTQ2016-77558-R).

■ REFERENCES

(1) (a) Cockroft, S. L.; Hunter, C. A. *Chem. Soc. Rev.* **2007**, *36*, 172. (b) Karshikoff, A. *Non-Covalent Interactions in Proteins*; Imperial College Press: London, 2006. (c) Raynal, M.; Ballester, P.; Vidal-Ferran, A.; van Leeuwen, P. W. N. M. *Chem. Soc. Rev.* **2014**, *43*, 1660. (d) Salonen, L. M.; Ellermann, M.; Diederich, F. *Angew. Chem., Int. Ed.* **2011**, *50*, 4808.

(2) (a) Burley, S.; Petsko, G. *Science* **1985**, *229*, 23. (b) Gallivan, J. P.; Dougherty, D. A. *Proc. Natl. Acad. Sci. U. S. A.* **1999**, *96*, 9459. (c) Meyer, E. A.; Castellano, R. K.; Diederich, F. *Angew. Chem., Int. Ed.* **2003**, *42*, 1210.

(3) (a) Wheeler, S. E. *Acc. Chem. Res.* **2013**, *46*, 1029. (b) Wheeler, S. E.; Houk, K. N. *J. Am. Chem. Soc.* **2009**, *131*, 3126.

(4) (a) Cockroft, S. L.; Hunter, C. A.; Lawson, K. R.; Perkins, J.; Urch, C. J. *J. Am. Chem. Soc.* **2005**, *127*, 8594. (b) Cockroft, S. L.; Perkins, J.; Zonta, C.; Adams, H.; Spey, S. E.; Low, C. M. R.; Vinter, J. G.; Lawson, K. R.; Urch, C. J.; Hunter, C. A. *Org. Biomol. Chem.* **2007**, *5*, 1062. (c) Hunter, C. A.; Low, C. M. R.; Rotger, C.; Vinter, J. G.; Zonta, C. *Proc. Natl. Acad. Sci. U. S. A.* **2002**, *99*, 4873. (d) Mati, I. K.; Cockroft, S. L. *Chem. Soc. Rev.* **2010**, *39*, 4195.

(5) Padial, J. S.; de Gelder, R.; Fonseca Guerra, C.; Bickelhaupt, F. M.; Mecinović, J. *Chem. - Eur. J.* **2014**, *20*, 6268.

(6) Annunziata, R.; Benaglia, M.; Cozzi, F.; Mazzanti, A. *Chem. - Eur. J.* **2009**, *15*, 4373.

(7) Duttwyler, S.; Do, Q.-Q.; Linden, A.; Baldridge, K. K.; Siegel, J. S. *Angew. Chem., Int. Ed.* **2008**, *47*, 1719.

(8) Chen, C.-T.; Siegel, J. S. *J. Am. Chem. Soc.* **1994**, *116*, 5959.

(9) (a) Ballistreri, F. P.; Maccarone, E.; Mamo, A. *J. Org. Chem.* **1976**, *41*, 3364. (b) Biggs, A. I.; Robinson, R. A. *J. Chem. Soc.* **1961**, 388. (c) Gross, K. C.; Seybold, P. G. *Int. J. Quantum Chem.* **2000**, *80*, 1107. (d) Gross, K. C.; Seybold, P. G.; Peralta-Inga, Z.; Murray, J. S.; Politzer, P. *J. Org. Chem.* **2001**, *66*, 6919. (e) Grunwald, E.; Ceska, G. W. *J. Am. Chem. Soc.* **1967**, *89*, 1377. (f) Pratt, D. A.; DiLabio, G. A.; Mulder, P.; Ingold, K. U. *Acc. Chem. Res.* **2004**, *37*, 334. (g) Pratt, D. A.; DiLabio, G. A.; Valgimigli, L.; Pedulli, G. F.; Ingold, K. U. *J. Am. Chem. Soc.* **2002**, *124*, 11085. (h) Vaschetto, M. E.; Retamal, B. A. *J. Phys. Chem. A* **1997**, *101*, 6945. (i) Vlasov, V. M. *J. Phys. Org. Chem.* **2009**, *22*, 756.

(10) Meot-Ner, M.; Deakyne, C. A. *J. Am. Chem. Soc.* **1985**, *107*, 474.

(11) Pandey, M. M.; Jaipal, A.; Kumar, A.; Malik, R.; Charde, S. Y. *Spectrochim. Acta, Part A* **2013**, *115*, 887.

(12) CCDC 1545154 and 1545155 contain the supplementary crystallographic data for this paper.

(13) (a) *Software for Chemistry & Materials*; http://www.scm.com, 2017. (b) te Velde, G.; Bickelhaupt, F. M.; Baerends, E. J.; Fonseca Guerra, C.; van Gisbergen, S. J. A.; Snijders, J. G.; Ziegler, T. *J. Comput. Chem.* **2001**, *22*, 931.

(14) (a) Becke, A. D. *Phys. Rev. A: At., Mol., Opt. Phys.* **1988**, *38*, 3098. (b) Johnson, B. G.; Gill, P. M. W.; Pople, J. A. *J. Chem. Phys.* **1993**, *98*, 5612. (c) Lee, C.; Yang, W.; Parr, R. G. *Phys. Rev. B: Condens. Matter Mater. Phys.* **1988**, *37*, 785. (d) van Lenthe, E.; Baerends, E. J.; Snijders, J. G. *J. Chem. Phys.* **1994**, *101*, 9783. (e) Russo, T. V.; Martin, R. L.; Hay, P. J. *J. Chem. Phys.* **1994**, *101*, 7729. (f) van Lenthe, E.; van Leeuwen, R.; Baerends, E. J.; Snijders, J. G. *Int. J. Quantum Chem.* **1996**, *57*, 281.

(15) Klamt, A. *J. Phys. Chem.* **1995**, *99*, 2224.

(16) Wheeler, S. E. *J. Am. Chem. Soc.* **2011**, *133*, 10262.

(17) (a) Daze, K. D.; Hof, F. *Acc. Chem. Res.* **2013**, *46*, 937. (b) Dougherty, D. A. *Science* **1996**, *271*, 163. (c) Dougherty, D. A. *Acc. Chem. Res.* **2013**, *46*, 885. (d) Kamps, J. J. A. G.; Huang, J.; Poater, J.; Xu, C.; Pieters, B. J. G. E.; Dong, A.; Min, J.; Sherman, W.; Beuming, T.; Matthias Bickelhaupt, F.; Li, H.; Mecinović, J. *Nat. Commun.* **2015**, *6*, 8911. (e) Kamps, J. J. A. G.; Khan, A.; Choi, H.; Lesniak, R. K.; Brem, J.; Rydzik, A. M.; McDonough, M. A.; Schofield, C. J.; Claridge, T. D. W.; Mecinović, J. *Chem. - Eur. J.* **2016**, *22*, 1270. (f) Ma, J. C.; Dougherty, D. A. *Chem. Rev.* **1997**, *97*, 1303. (g) Salonen, L. M.; Holland, M. C.; Kaib, P. S. J.; Haap, W.; Benz, J.; Mary, J.-L.; Kuster, O.; Schweizer, W. B.; Banner, D. W.; Diederich, F. *Chem. - Eur. J.* **2012**, *18*, 213. (h) Schärer, K.; Morgenthaler, M.; Paulini, R.; Obst-Sander, U.; Banner, D. W.; Schlatter, D.; Benz, J.; Stihle, M.; Diederich, F. *Angew. Chem., Int. Ed.* **2005**, *44*, 4400.

(18) (a) Bickelhaupt, F. M.; Diefenbach, A.; de Visser, S. P.; de Koning, L. J.; Nibbering, N. M. M. *J. Phys. Chem. A* **1998**, *102*, 9549. (b) Wolters, L. P.; Bickelhaupt, F. M. *WIRES Comput. Mol. Sci.* **2015**, *5*, 324.

(19) Fonseca Guerra, C.; Handgraaf, J.-W.; Baerends, E. J.; Bickelhaupt, F. M. *J. Comput. Chem.* **2004**, *25*, 189.

DOI: 10.1021/acs.joc.7b01406
J. Org. Chem. 2017, 82, 9418−9424